The Stability of Phase-locked Oscillators and the Measurement of Allan Deviation

Bill Slade
Orban Microwave Products
http://www.orbanmicrowave.com

May 8, 2013

Abstract

In our highly connected society, the ability to precisely synchronize many remote clocks and oscillators to primary (atomic) frequency references is indispensible for commercial, scientific, medical and everyday personal uses such as navigation and digital broadcasting [1]. The quality of these services depends heavily on the precise tracking of the atomic reference by the phase-locked local oscillator (often in a low carrier to noise environment).

In this paper, we review some of the theoretical background of phase locked oscillators and the definition of Allen deviation (ADEV) as well as why the usual phase error definition is inadequate. Some of the common existing measurement methods are reviewed as well as an outline of the approach used in our measurements. We then verify the method by providing the example of a precision Doppler measurement (like what one might see in a deep space radio science experiment) and how ADEV provides a way to quantify errors in the scientific results.

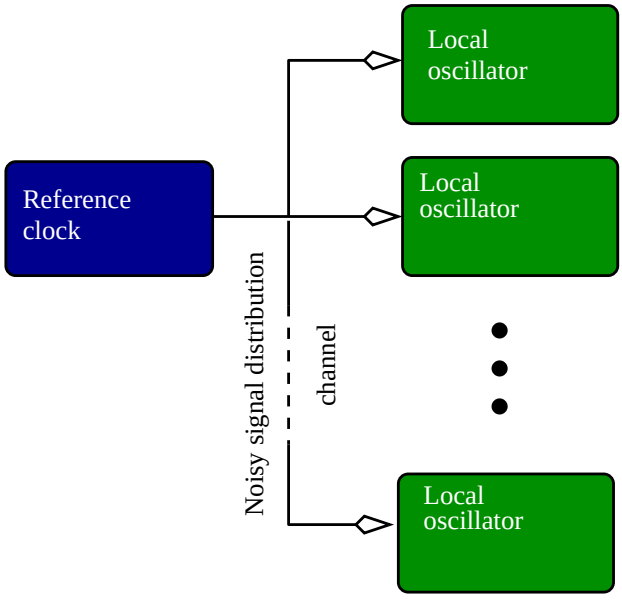

Figure 1: Clock distribution by means of a chain of secondary phase locked oscillators locked to a primary reference.

1 The phase-locked oscillator

Phase locked oscillators are an ubiquitous, indispensible technology. Their usefulness stems from the fact that many applications require the frequency stability of a high quality oscillator, but cost or size limitations prohibit the local use of a primary frequency reference (such as a cesium clock). Hence, we lock our low-cost, small local oscillators to a signal generated by the primary source (Figure 1). For example, using a GPS signal (which is referenced to an ensemble of cesium and/or hydrogen masers), our local oscillator will acquire the long-term stability of the reference clock ensemble.

Another example is a deep-space Doppler transponder that "listens" to an uplink tone from Earth that is generated from a high-quality reference clock. The transponder local oscillator tracks the uplink tone using classical phase-locking techniques, thereby acquiring the long-term stability characteristics of the ground-station clock. As a result, any residual frequency shifts observed on the return link will be due to Doppler shifts from relative motion between the transponder and the ground station.

The usual definition of phase noise is not very useful in quantifying the long-term phase and frequency errors encountered in time-critical applications such as Doppler measurements and precision navigation, where even a single "cycle slip" in a local oscillator can introduce significant error. Allan Deviation pro-

vides a way to include long-term, cumulative phase errors. This paper will provide a brief tutorial on the concept of frequency stability and Allan deviation in phase-locked oscillators as well as present methodology for ADEV measurement that is somewhat different from the traditional measurement methods seen in the precision timekeeping literature. An example measurement of a deep-space Doppler transponder is presented as well.

1.1 Model of carrier tracking loop

In order to adequately model a frequency tracking loop that locks to a noisy reference, we need to define the loop topology as well as an adequate model of the noisy reference signal. Figure 2 shows the models for the reference signal noise as well as the tracking loop model.

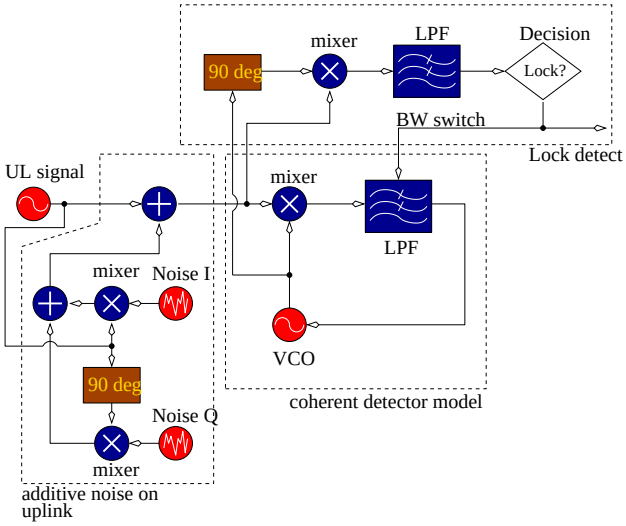

Figure 2: Illustration of uplink reference signal noise model with tracking loop model.

The reference signal is represented as

$$r(t) = \cos(\omega_r t), \tag{1}$$

where $\omega_r t$ is the instantaneous phase of the uplink signal (product of angular frequency and time, respectively). The reference signal is contaminated with narrowband additive gaussian noise on the in-phase and quadrature channels and down converted by the local oscillator signal (the VCO).

The local oscillator (which acquires and tracks the reference tone) is represented in terms of its own instantaneous phase ϕ_l as

$$s(t) = \cos\phi_l. \tag{2}$$

The full signal (reference signal + noise) seen by the coherent detector tracking loop is

$$r_n(t) = (1 + n_i(t))\cos(\omega_r t) - n_q(t)\sin(\omega_r t), \tag{3}$$

given the independent bandlimited gaussian noise sources $n_i(t), n_q(t)$.

After downconversion, the uplink signal is given by (showing only the difference frequency terms, since the low-pass filter is assumed to remove the sum-frequency components):

$$r_d(t) = \frac{1}{2}\{(1 + n_i(t))\times \cos(\omega_r t - \phi_l) + n_q(t)\sin(\omega_r t - \phi_l)\}. \tag{4}$$

The tracking loop low-pass filter is based on the common lead-lag RC low-pass filter shown in Figure 3.

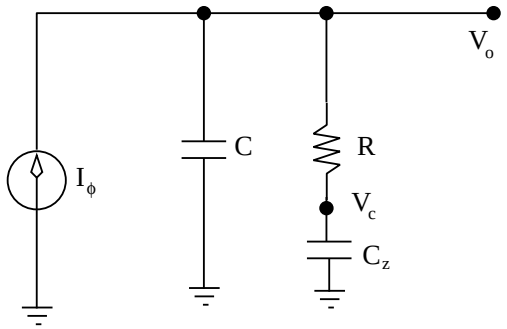

Figure 3: The lead-lag integrating filter driven by a current output I_ϕ from the phase detector and producing the VCO tuning voltage V_O. V_c is needed for the filter circuit model.

The phase detector is based on a simple multiplier whose current output depends on the product of uplink signal and the local oscillator signal "voltages." If we normalize the signal input and assume a mixer gain of K_ϕ, the current source driving the loop filter depends on

$$I_\phi = K_\phi \left(\frac{1 + n_i(t)}{\sqrt{1+\sigma_N^2}} \cos(\omega_r t - \phi_l) + \frac{n_q(t)}{\sqrt{1+\sigma_N^2}} \sin(\omega_r t - \phi_l) \right\}. \tag{5}$$

The signal levels are normalized to simulate the effect of a non-coherent AGC. The variable σ_N^2 is the noise variance that is used to set the carrier-to-noise ratio. The uplink sinusoid is assumed to have a constant value of unity.

The set of equations that define the dynamics of acquisition and tracking are then written as

$$\dot{V}_O = \frac{1}{C} I_\phi - \frac{V_O - V_c}{RC} \quad (6)$$

$$\dot{V}_c = \frac{V_O - V_c}{RC_z} \quad (7)$$

$$\dot{\phi}_l = K_{\text{VCO}} V_O + f_0. \quad (8)$$

The system of equations are integrated subject to a user chosen set of initial conditions (usually zero) and the initial local oscillator frequency f_0 chosen not too far from the uplink carrier frequency (within the capture range of the loop). When $CNR = 1/2\sigma_N^2$ is 2.9 dB and the loop bandwidth is near 2300Hz, the lockup and tracking dynamics are clearly visible in the plot of the phase detector output (error) signal in Figure 4. The error signal starts showing

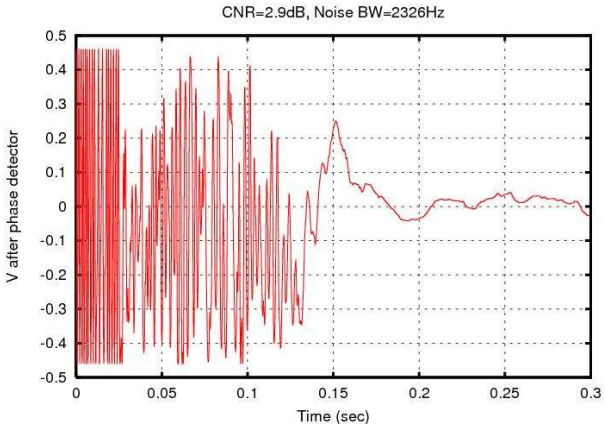

Figure 4: Illustration of lockup and tracking when the CNR is set to a level just above that where lockup is guaranteed to occur within 0.1 second with about a 1kHz initial frequency offset in the local oscillator.

the effects of strong pull-in of the vco toward the reference frequency around 0.025 seconds. The resultant cycle slipping is seen until lock is achieved near 0.125 seconds. Beyond this, there is no more cycle slipping, but error signal varies randomly as a result of the loop correcting for the phase variations caused by the noise on the uplink reference signal. If we measure the instantaneous frequency once lock is achieved, is will display characteristics of a zero-mean process (as will the phase difference between the local oscillator and the reference). There will be no relative frequency drift. In this case, the usual phase noise relationships can be used to estimate the long-term stability of the phase locked oscillator.

If the CNR is reduced, slightly below the threshold for reliable tracking, cycle slips are frequent and lock is never fully achieved (Figure 5). In Figure 5, cycle

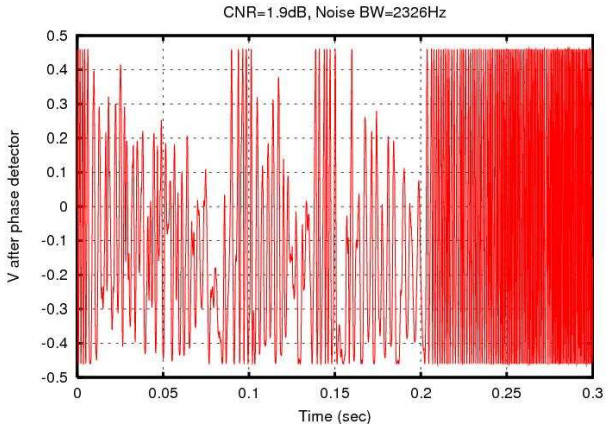

Figure 5: Illustration of a situation where lock is never achieved. CNR=1.9dB, Noise BW=2.3kHz.

slipping is observed around 0.01 sec until about 0.075 seconds when lock is momentarily achieved. However, the noise level is too high to permit lock to be maintained. The local oscillator slips out of lock and the cycle slipping process begins again. Eventually, the local oscillator "runs away" completely around 0.2 seconds and lock is impossible. In this case, the frequency and phase processes cannot be defined using the usual statistics. If frequency tracking is lost, the instantaneous frequency is no longer represented by a zero-mean process and, in fact, an unbiased estimator for average frequency or its variance cannot be found since any estimate will depend on the length of the data set.

1.2 Tracking and probability of cycle slips

Under most practical situations, the CNR is high enough that cycle slips should be rare events. The uplink noise that is impressed on the local oscillator will be reduced by the action of the frequency steering loop. The phase error variance can be estimated by

$$\sigma_\phi^2 \approx \frac{1}{CNR}. \quad (9)$$

This implies an expression of a normal probability density function in terms of the phase random variable ϕ [2].

$$P(\phi) = \frac{1}{\sqrt{2\pi}\sigma_\phi} \exp(-\phi^2/2\sigma_\phi^2). \quad (10)$$

A cycle slip occurs when the phase exceeds the $[-\pi, \pi]$ range in any given cycle (assuming we sample

once every expected cycle time). The probability of a slip in any cycle is approximated by

$$Pr(|\phi| > \pi) = \text{erfc}\left(\frac{\pi}{\sigma_\phi\sqrt{2}}\right). \quad (11)$$

Using the model of Bernoulli trials [3], the probability of k cycles slipping in n observed cycles is

$$Pr(k \text{ slips in } n \text{ observed cycles} = \frac{n!}{k!(n-k)!}(Pr(|\phi| > \pi)^k \times (1 - Pr(|\phi| > \pi))^{n-k}. \quad (12)$$

The probability of no cycle slips in n cycles is given by setting $k = 0$:

$$Pr(\text{no slips registered}) = (1 - Pr(|\phi| > \pi))^n. \quad (13)$$

It is convenient to consider the logarithm of the probability and include the relationship $n = f_r\tau$ (f_r is uplink frequency in Hz and τ is the observation period in seconds). Hence, we see that

$$\log_{10} Pr(\text{no slips registered}) \approx -\frac{f_r\tau}{\log 10}\text{erfc}\left(\frac{\pi}{\sqrt{2}}\sqrt{CNR}\right). \quad (14)$$

For an uplink signal frequency of 7.162GHz, Figure 6 depicts the log probability of no cycle slips for 10, 60 and 1000 second observation periods. This plot allows us to put a limit on the CNR such that we are fairly sure that no frequency errors due to cycle slips will be observed in these time periods.

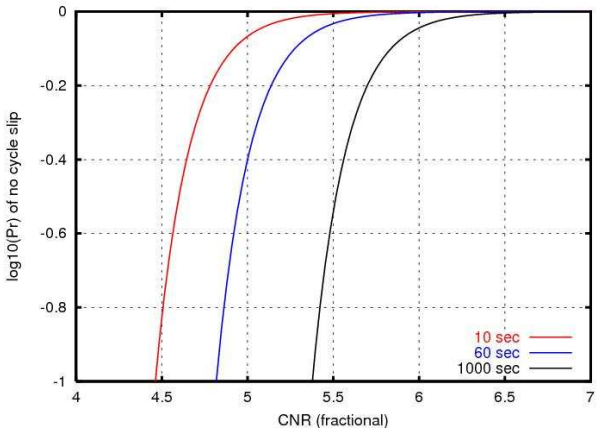

Figure 6: Log probability of observing no cycle slips within 10, 60 or 1000 seconds versus uplink CNR. Vertical axis value of -0.3 is roughly the point where a slip is 50% likely in the observation period.

The respective fractional (not dB) CNR values for even odds of a cycle slip occurring are 4.7, 5.1 and 5.7 for 10, 60 and 1000 second observation times.

Note that we have relied on a linear phase tracking assumption (PLL is locked) and we assume that cycle slipping events are independent of each other (generally not true, because cycle slips imply a loss of lock and often occur in bursts; a violation of the assumptions in this argument). However, if we assume that cycle slip events are "rare," for large CNRs, this model should be reasonably valid.

A full non-linear treatment would require solutions to the Chapman-Kolmolgorov or Fokker Planck equations [4]. For first and second order tracking loops, mean time between cycle slips can be estimated using the expression from:

$$T_m = \frac{\pi^2 I_0(CNR)\cdot CNR}{2B_l}. \quad (15)$$

$I_0()$ is the zero-order modified Bessel function. For third-order loops (like the one discussed here), closed form expressions do not exist, but (15) can be used for order-of-magnitude estimates. In fact, (15) indicates a 50% chance of slips for fractional CNR = 3.0, 3.9 and 5.3 for the respective observation times. This is a reasonable confirmation of our simple probabilistic model.

2 Concept of frequency stability

The fundamental output of an oscillator can be expressed as [5]

$$V(t) = (A + \epsilon(t))\cos(\phi(t)), \quad (16)$$

where A is the signal amplitude and $\epsilon(t)$ represents small amplitude perturbations. Of most interest in frequency stability and coherence is the time-dependent phase $\phi(t)$ (already introduced in the preceding section on phase locking). The phase is given by

$$\phi(t) = 2\pi f_0 t + \varphi(t), \quad (17)$$

where f_0 is the nominal frequency of the "perfect" signal and $\varphi(t)$ is the phase deviation (as a result of phase noise and frequency drift). We shall define the instantaneous **fractional frequency deviation** to be

$$y(t) = \frac{\Delta f}{f_0} = \frac{1}{2\pi f_0}\frac{d\varphi}{dt}. \quad (18)$$

If we sample $y(t)$ at discrete, equispaced time instants, we will have a time series of fractional frequency deviations y_i.

2.1 Standard phase noise variance

By applying the definition of standard N-point variance [5], [6],

$$\sigma_y^2 = \frac{1}{N-1}\sum_{i=0}^{N}(y_i - \overline{y})^2\,, \tag{19}$$

we can achieve some kind of quality measure of our signal. For anything other than bandlimited zero-mean phase noise, this definition will not converge to a finite number as the sample length tends to infinity. For this reason, the standard variance should not be used for general frequency stability measurements. However, it can still be useful for measurements where a frequency comparison between coherent (phase-locked) oscillators is desired.

The usual way of representing the standard phase-noise variance is

$$\sigma_\varphi^2 = \frac{1}{(M-2)T_s^2M^2}\sum_{m=1}^{M}(x_m - \overline{x})^2\,, \tag{20}$$

where x_i is the bandlimited phase error given by the integral (or in the discrete case, the sum) over the frequency deviation:

$$x_i = 2\pi f_0 T_s \sum_{n=1}^{i} y_n \tag{21}$$

and $\overline{x}$ is the average phase over all sampled points and T_s is the sampling period, f_0 is the signal center frequency. This phase error variance is the one usually related to the carrier-to-noise ratio of the signal (see expression (9)) from which the frequency-time series is computed. The expression (21) is, in reality, nothing more than the integral over time of the fractional frequency deviation. It is generally not a valid estimator if the fractional frequency deviation random samples y_n are not governed by a zero mean process.

Conventional phase noise measurements usually use phase locked methods to eliminate frequency/phase drift between the device under test and the phase noise meter and hence the standard phase noise variance is still valid. If there are "cycle-slips" between the phase-locked oscillator and its frequency standard, a phase noise meter will miss these events and standard noise variance is no longer applicable, because now there is the possibility of unbounded phase drift.

2.2 The overlapping Allan variance

Let us now look at a better way to quantify frequency/phase errors: the Allan variance (or Allan deviation). If we integrate the frequency time series, we generate a series whose values represent a normalized phase as time (index i) progresses:

$$x_i = 2\pi f_0 T_s \sum_{n=1}^{i} y_n + x_0. \tag{22}$$

The overlapping AVAR is defined as

$$\sigma_y^2(\tau) = \frac{1}{4\pi(M-2m+1)f_0^2\tau^2} \sum_{i=1}^{M-2m+1}(x_{i+2m} - 2x_{i+m} + x_i)^2\,, \tag{23}$$

where M is the size of the total measurement data set, m is the "stride" and is related to the length of the overlapping integration periods by $\tau = mT_s$ (see Figure 7). This is the definition we use here and is the one accepted as yielding a good quality estimator for AVAR [5].

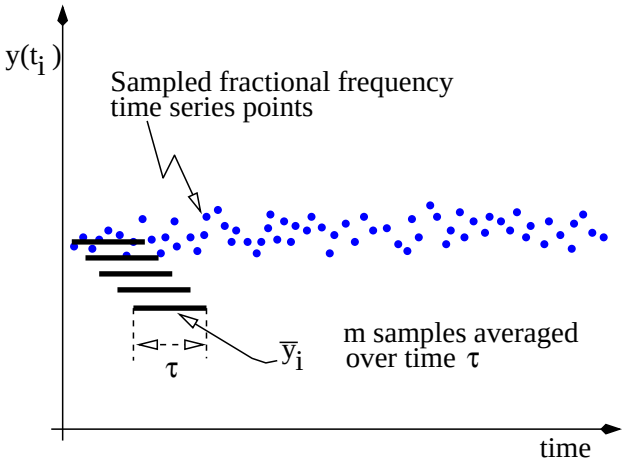

Figure 7: Illustration of how the average frequency deviation is generated over the sampled frequency points in the time series. Each average $\overline{y}_m$ is carried out over overlapping blocks of frequency samples.

It is interesting to observe that the definition of he AVAR statistic is based on a classical centered difference definition of the second derivative of phase with respect to time. In other words, AVAR is, loosly

speaking, a measure of the curvature of the phase function versus time. If the phase evolves along a perfect straight line with respect to time, we have perfect frequency stability and AVAR will vanish. In reality, however, the phase function will exhibit jitter as well as possible overall trends that will deviate from the ideal. This is what AVAR quantifies.

2.3 Precision frequency metrology and deep-space Doppler velocity measurements

With the exploration of the solar system (and beyond), Doppler measurements of space probe velocities and planetary movements have become common. The process usually involves transmitting a highly frequency stable (i.e. locked to a precision atomic standard) uplink (UL) radio signal from an Earth ground station toward a coherent transponder on board of the spacecraft or planetary lander. The coherent transponder phase-locks to the UL signal, thereby acquiring the long-term coherence of the atomic frequency standard on Earth. However, since the Earth and the space-borne transponder are moving relative to one another, the uplink signal is Doppler shifted with respect to the original Earth station frequency. Therefore, the coherently-locked transponder local oscillator tracks the Doppler shift on the UL signal. The transponder local oscillator is used to generate a coherent downlink (DL) signal that is transmitted back to Earth. The receiver at the Earth ground station measures the frequency of the returning signal. The received DL signal frquency f_{DL} is compared to the expected return DL "no-motion" frequency f_0 to extract the relative velocity v_r using

$$v_r = \frac{c}{2}\frac{(f_{DL} - f_0)}{f_0}, \tag{24}$$

where c is the speed of light and $v_r << c$. Note that the measured velocity is that along a line connecting the "line-of-sight" between the ground station and the transponder. Velocity components transverse to the line-of-sight do not contribute to Doppler shift (see Figure 8).

Good results in Doppler metrology rely on the ability of the transponder to track the uplink tone with absolute precision (no cycle slips of other frequency disturbances). The transponder ADEV is important in this measurement because it can give a lower bound on the theoretical error of the Doppler measurement link. (There are, of course, other factors like DL noise [7], mechanical disturbance, scintillation effects

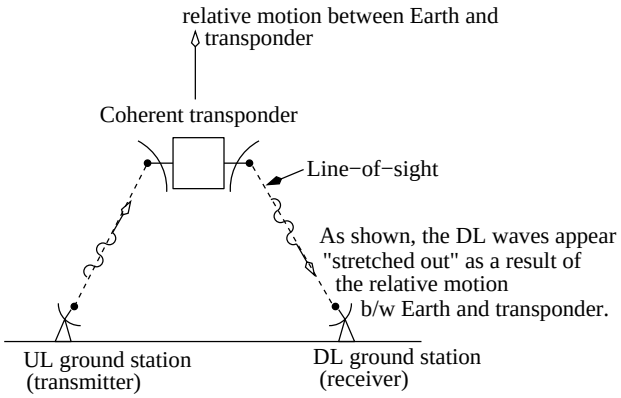

Figure 8: Simplified illustration of Doppler link. Only velocity components along the lines of sight contribute to Doppler shift.

[8], [9], etc.) The fractional error in the Doppler frequency measurement is given by the ADEV and hence the velocity errors are directly related by

$$\sigma_v(\tau) = \frac{c}{2}\sigma_A(\tau). \tag{25}$$

Doppler velocity information is extracted by integrating the received DL frequency over fairly long periods (τ = 10-1000 seconds). This has the effect of reducing the effect of phase noise on the measurement. If the tranponder DL signal never loses coherence (never slips cycles), longer integration times will yield progressively more precise values for the Doppler velocity. If the ADEV is large, it takes a long time to achieve a specified Doppler precision (usually less than 1mm/sec). If ADEV is small, the desired Doppler precision can be achieved over shorter integration times. This is of practical importance for ground stations that are tracking many space missions and scientific results must be collected over the shortest possible observation times.

3 Measuring AVAR/ADEV

3.1 Estimating AVAR from noise spectral density

When characterising an oscillator that is phase-locked to a master clock that is, in turn, common to the measurement apparatus, phase noise can be estimated from the oscillator noise spectral density (based on the usual noise variance and measurement bandwidth, of course). In effect, we can carry out a phase noise measurement on the oscillator under test

and estimate the AVAR from

$$\sigma_A = \frac{\sqrt{3}}{2\pi f_0 \tau} \cdot \frac{1}{\sqrt{2 \cdot CNR}}, \tag{26}$$

where CNR is the band-limited carrier to noise ratio of the test oscillator as determined from a standard phase noise measurement over a signal bandwidth BW (usually determined by filters in the receiver). This expression comes from integrating the phase-noise spectral density "filtered" by the time-averaging of frequency over the rectangular time window τ:

$$\sigma_A^2 = \int_0^{BW} S_y(f) \frac{\sin^4(\pi f \tau)}{(\pi f \tau)^2} df, \tag{27}$$

given the frequency time-series spectral density is estimated as $S_y(f) = f^2 N_0 / f_0^2$ and N_0 is the oscillator average noise spectral density.

This technique allows the estimation of AVAR using standard laboratory instruments (spectrum analyser and laboratory oscillators). Estimating ADEV from phase-noise spectral density results is a convenient way to generate results for confirming time domain measurements **as long as cycle slips are not encountered**.

3.2 Time-domain measurement of ADEV

We now focus on some time-domain methods of extracting AVAR/ADEV. There are several methods that have been established to measure frequency (and thereby, the AVAR/ADEV) in the time domain. Perhaps the most straightforward is to use a time-interval counter to compare the zero-crossing times of two oscillators [5]. Phase and frequency errors are then deduced from variations in the jitter found at the zero-crossings. The drawback incurred by this method is the need for a high-speed precision interval counter. This requirement can be overcome to a large extent (if not entirely) using other methods.

One such technique is the Heterodyne Method, where the clock frequency is translated to some lower frequency using a frequency mixer. In this way, high resolution frequency deviation measurements can be achieved using an ordinary (not high speed) period counter. Jitter and drift in zero-crossings of this "downconverted" clock signal are then translated into the desired AVAR data. Care must be taken to establish the drift direction.

The Dual Mixer Time Difference method combines the best aspects of the two previous measurement methods by comparing the relative phase of the beat signals of a pair of mixers driven by a common reference frequency and an offset that is locked to the common reference. All of these methods are described in some detail in [5], so we shall not delve into these methods deeply here.

On the other hand, we wish to describe a method similar to the Heterodyne Method that allows measurements of instantaneous phase and frequency without the need for interval counters. Since we need to measure the phase/frequency properties of a signal in X-band (8.415 GHz), it makes sense to look at the AVAR measurement system from a radio-engineering point-of-view (direct phase measurement), instead of a timing perspective (zero-crossings).

It is well known that mixers preserve the phase difference between two signals (an RF and local oscillator signal, for example). This fact can be used to construct a radio that receives the 8.415GHz signal and produces output signals that are proportional to the band-limited instantaneous phase difference between the receiver local oscillator and the input signal (the DL signal from the transponder we wish to measure). The proposed transponder AVAR measurement system based on this method has the block diagram shown in Figure 9.

To make this method work, we need to formalise some of the details for extracting phase and frequency from a down-converted radio signal.

3.3 Extracting phase and frequency information from I and Q signals

The output baseband I and Q signals are related to the difference in phase between the input RF signal and the local oscillator $\phi = \phi_{RF} - \phi_{LO}$:

$$I = A\cos(\phi), \tag{28}$$

$$Q = A\sin(\phi). \tag{29}$$

A is an arbitrary amplitude factor defined by the setting of the AGC level. The phase difference between the uplink signal and the local oscillator tone is

$$\phi = \arctan\left(\frac{Q}{I}\right) \tag{30}$$

The instantaneous frequency at any time point is defined as the time derivative of the phase. Differentiating (30) with respect to time yields measured f in terms of the baseband signals I and Q:

$$f_{meas} = \frac{1}{2\pi\left(I^2 + Q^2\right)}\left(I\frac{dQ}{dt} - Q\frac{dI}{dt}\right). \tag{31}$$

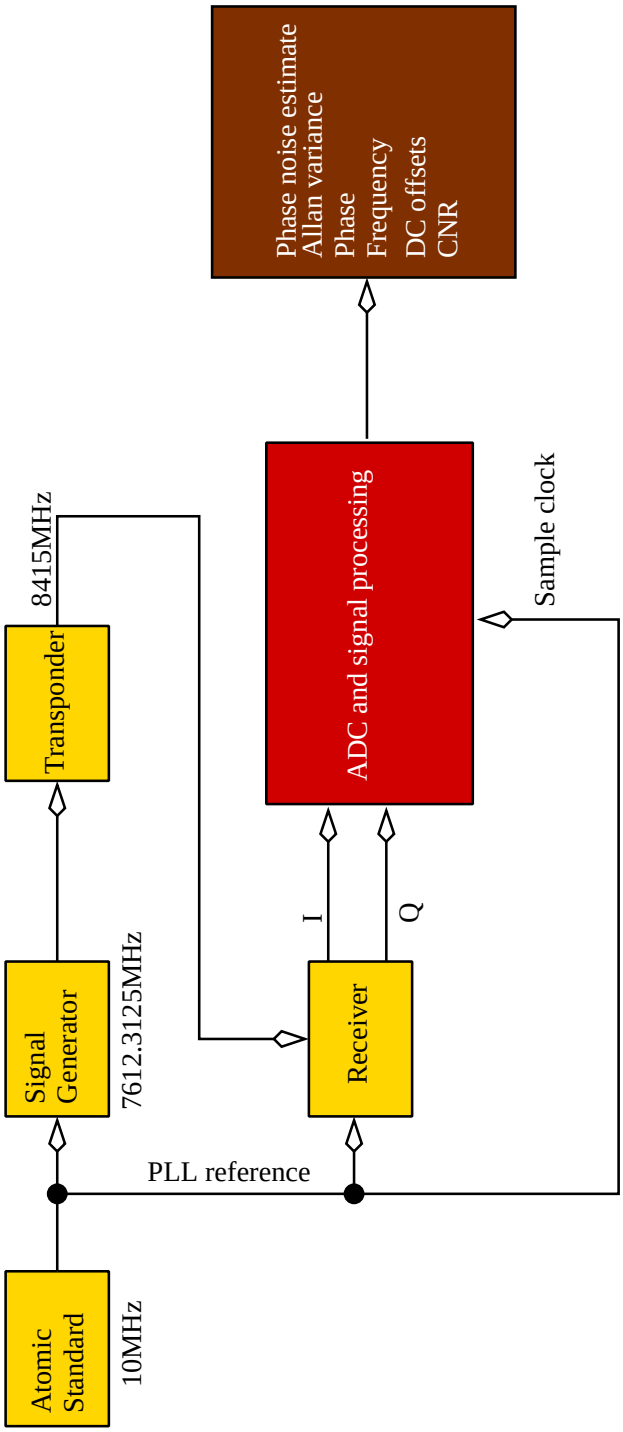

Figure 9: Transponder AVAR measuring system.

This is an extremely convenient expression because it allows the acquisition of measurement data in its rawest form (samples of I and Q) with a minimum of preliminary signal processing (like that performed by zero-crossing detectors and interval counters used in traditional frequency analysis). Frequency determination is done in software, using (31) directly in the I and Q samples. In addition, this method is capable of handling both positive and negative frequency deviations without the need for extra processing (as is the case with the simple Heterodyne Method described above).

The downconversion scales all frequency deviation effects into the audio range, meaning that extremely high resolution phase and frequency measurements can be carried out using relatively low-cost sampling hardware and simple software tools. Furthermore, complex spectral analysis and adaptive digital filtering can be used to enhance signal detection and frequency determination directly on the I and Q samples. In fact, the effects of very narrow band DL receivers can be easily constructed in the digital domain, which would otherwise be very difficult, if not impossible to construct using analog circuits.

After generating the frequency time-series, ADEV is easily evaluated using (23).

3.4 The AVAR of the device-under-test

Since the measurement system is not a perfectly noiseless system, it contributes to the overall measured AVAR. Fortunately, the total system AVAR follows the "sum of variances" rule :

$$\sigma^2_{A\ system} = \sigma^2_{A\ DUT} + \sigma^2_{A\ test\ system}. \qquad (32)$$

By performing a measurement of AVAR on the measurement system without the DUT, we can establish an estimate for $\sigma^2_{test\ system}$. Then, by performing a measurement with the DUT (transponder) in place, we generate σ^2_{system}. A simple difference between the AVARs yielded by these two measurements gives us an estimate for the transponder AVAR.

3.5 An example measurement

To verify the test platform in Figure 9, the ADEV of a coherent transponder breadboard was measured after characterising the test system. The test conditions and some pertinent specifications of the transponder are shown in Table 1.

The DL frequency is 8 415 000 094 Hz. This means that the UL center frequency must be 7 162 312 580 Hz, since the transponder DL/UL frequency turnaround ratio is 880/749. The UL signal level

Parameter	Value	Units
UL frequency	7.162	GHz
DL frequency	8.415	GHz
UL signal level	-100	dBm
UL freq. offset	80	Hz
Transponder ratio	880/749	–
DL signal level	-60	dBm
Resulting DL freq. offset	93.99	Hz
ADC sample rate	10.0	kHz
ADC resolution	10	bits
AVAR test set BW	2.5	kHz
Test set anti-alias LPF order	6 Butterworth	–

Table 1: The test conditions used for the ADEV measurement.

is chosen such that oscillator noise in the transponder will dominate (instead of thermal noise on the UL signal). Artificial noise (a pseudo-noise chip sequence) is added on the uplink quadrature channel to simulate the effects of uplink noise. The AVAR test set receiver local oscillator is fixed to 8.415GHz. The resultant 94 Hz shift is clearly evident in spectral plot in Figure 10.

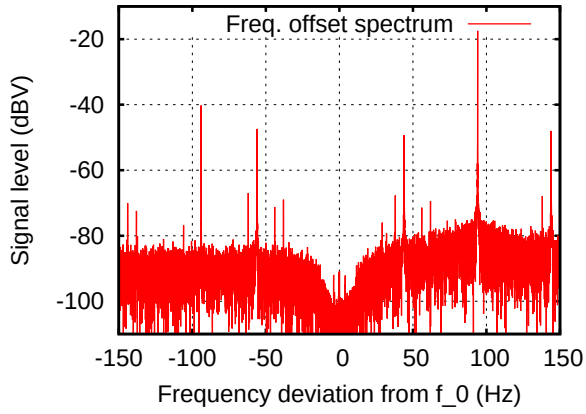

Figure 10: AVAR receiver output spectrum showing +94Hz tone (highest peak on right). Other peaks arise from distortion effects and imperfect image cancellation.

Samples of the I and Q outputs are taken over a 20 minute sampling session at 10000 samples/second (sample clock also locked to atomic reference). This gives a set of approximately 2^{23} samples, on which we perform the ADEV calculation (as well as the spectral analysis in the preceding illustration), producing the results in Figure 11.

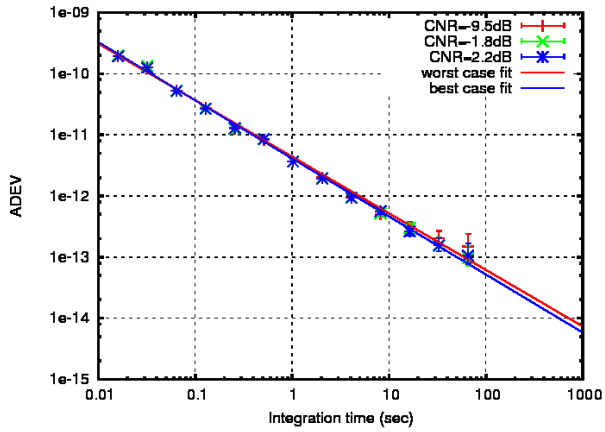

Figure 11: Results of an ADEV measurement on the full system, including the coherent transponder. Straight line fits show trends of for best and worst case CNRs (2.2dB, -9.5dB; RBW=10kHz).

The ADEV represents an estimate of the fractional frequency error, hence an estimate of the upper bound of the Doppler measurement precision can be computed using the expression in (25) (see Table 2).

Integration time	FD ADEV	TD ADEV	Doppler error
10 sec	8×10^{-13}	5×10^{-13}	7.5×10^{-2}
60 sec	2×10^{-13}	9×10^{-14}	1.3×10^{-2}
100 sec	8×10^{-14}	5×10^{-14}	7.5×10^{-3}
1000 sec	8×10^{-15}	6×10^{-15}	7.5×10^{-4}

Table 2: Comparison of ADEV calculated from frequency (FD) and time domain (TD) data for AVAR test receiver as well as Doppler errors (in mm/sec).

Good agreement is illustrated in Table 2 between the spectral density estimation of ADEV (FD-ADEV) and ADEV measured using the time-domain sampling apparatus developed as part of this work (TD-ADEV).

The ADEV curves in Figure 11 exhibit structure that gives clues to the types of noise that are present in the system. The test system ADEV (the red curve in Figure 11) follows a trend that indicates white/flicker phase noise as the dominant noise mechanism. This is because the slope is nearly -1, indicative of the τ^{-1} time-domain power law expected for this type of noise [5]. The errorbars indicate the region of the 95% confidence interval on the measurement.

To illustrate the effects of non-stationary noise events on the ADEV, observe the shape of the curve in Figure 12. In this case, slight mechanical disturbances

degrade the short-term stability of the full system (seen on a scale of 1-10sec) as observed by the flattening of the upper left of the transponder ADEV curve (black). Note the relatively straight-line decrease of the test system ADEV with integration time (as expected for system that maintains perfect phase-locking with the common frequency reference).

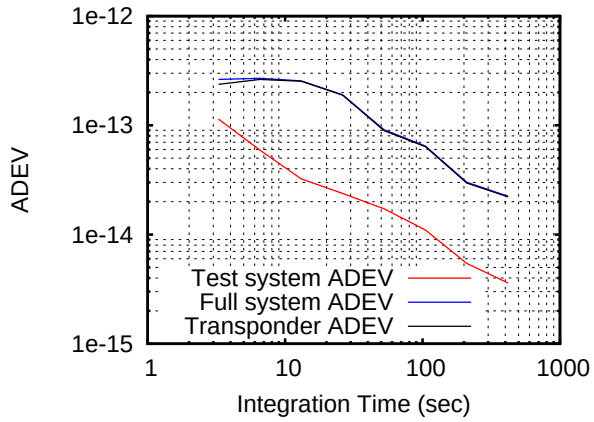

Figure 12: Results of an ADEV measurement where mechanical vibration disturbs the frequency stability of phase-locked oscillator.

4 Final words

In order to quantify the errors induced by cycle slip and other frequency errors in carrier-tracking receivers, we need to move away from the traditional idea of phase noise errors toward a more general statistical representation of timing errors in high frequency signals. ADEV provides one route, since it provides not only information on phase error, but provides a scale ranking of error events that gives clues to the type of noise present in the system.

We have developed a heterodyne downconversion system for measuring ADEV that avoids the need for high speed interval counters or multiple clocks. Software has been developed that extracts the instantaneous phase difference between the transponder downlink signal and a local oscillator locked to a common high quality frequency reference. The test system itself should generate no relative frequency drift, hence long-term frequency errors will be dominated by possible undesired frequency deviations (e.g. cycle slips) in the transponder tracking loop.

Tests indicate that good results can be obtained in a fairly straightforward fashion as long as care is taken to reduce confounding factors such as mechanical vibrations and temperature variations.

5 Corrections and Modifications to document

1. 20130508: Equations 21, 22 and 23 lacked factor of $2\pi f_0$. Added text.
2. 20130508: Equation 26 σ_A^2 changed to σ_A.

References

[1] D. W. Allan, N. Ashby and C. C. Hodge, *The Science of Timekeeping*, Hewlett-Packard App. Note 1289, 1997. (Available at `http://www.allanstime.com/Publications/DWA/Science_Timekeeping/index.html`).

[2] A. Blanchard, *Phase Locked Loops,* Wiley, 1976.

[3] G. R. Cooper, C. D. McGillem, *Probabilistic Methods in Signal and System Analysis*, Holt, 1971.

[4] L. Schuchman, "Time to cycle slip in first and second order phase lock loops," *NASA Tech. Memorandum 69-2034-8*, Dec. 19, 1969.

[5] W. J. Riley, *Handbook of Frequency Analysis,* NIST Time and Frequency Division, June 2008. (Can be found at `http://tf.nist.gov/timefreq/general/pdf/2220.pdf`)

[6] D. W. Allan, "Should the classical variance be used as a basic measure in standards metrology?" *IEEE Trans. Instrum. Meas.,* vol. IM36, pp. 646-654, 1987.

[7] P. W. Kinman, "34-m and 70-m Doppler," *Doc 810-005, Rev. E*, NASA-JPL, 2002.

[8] K. C. Yeh and C. H. Liu, "Radiowave Scintillations in the Ionosphere," *Proc. IEEE,* vol. 90, pp. 324-360, 1982.

[9] A. W. Wernik and J. C. Cerisier, "Radio Scintillation by Martian Turbulent Ionosphere and Atmosphere Simulation Results," *Proc. URSI GA02*, Paper 382, 2002. (Can be found at `http://ursi-test.intec.ugent.be/?q=node/8`).